Vortex localization in rotating clouds of bosons and fermions

S.M. Reimann[1], M. Koskinen[2], Y. Yu[1] and M. Manninen[2]
[2]*Mathematical Physics, LTH, Lund University, SE-22100 Lund, Sweden and*
[1]*NanoScience Center, Department of Physics, FIN-40014 University of Jyväskylä, Finland*

Finite quantal systems at high angular momenta may exhibit vortex formation and localization. These phenomena occur independent of the statistics of the repulsively interacting particles, which may be of bosonic or fermionic nature. We analyze the relation between vortex localization and formation of stable Wigner molecules at high angular momenta in the view of particle-hole duality. Trial wave functions for the vortex states and the corresponding fermion-boson relations are discussed.

PACS numbers: 03.75.Lm, 05.30.Fk, 73.21.La

I. INTRODUCTION

When small quantal systems are set rotating, vortices may form. These vortices are characterized by rotational flow of particle current around minima in the density distribution. In contrast to fluid mechanics, a vortex in a quantum system can be n-fold quantized, with the corresponding wavefunction having a (n-fold) zero at the vortex position and a phase changing by $n2\pi$ on a path around this zero.

The existence of a triangular vortex lattice in superconductors was predicted by Abrikosov [1] already in the 50ies. In the mesoscopic regime, finite-size effects determine the symmetry of multivortex configurations. In small systems, a compromise must be found between the triangular lattice of the bulk, and the shape of the confinement. It was predicted [2, 3, 4, 5] that on a small superconducting disk, instead of the triangular Abrikosov lattice, the vortices may form geometric patterns that resemble those of classical point charges in a harmonic potential, i.e. small, finite-size Wigner crystals or so-called Wigner molecules [6, 7]. This was experimentally confirmed very recently by Grigorieva *et al.* [8].

However, the appearance of vortices and their localization is not limited to superconductivity or superfluidity. Another well-known example is a Bose-Einstein condensate (BEC) of (repulsive) alkali-metallic atoms (see, for example, Dalfovo *et al.* [9] and Legett [10], or the book by Pethick and Smith [11] for reviews on BEC), which is set rotating. With increasing angular momentum, an ever larger number of vortices may penetrate the bosonic cloud of atoms [12, 13, 14].

In BEC, much work focused on the Thomas-Fermi regime of strong coupling [9, 15, 16, 17, 18, 19], where the kinetic energy dominates. In the dilute limit, however, even though the interactions are weak they play the major role [20, 21, 22, 23, 24, 25, 26]. Within the Gross-Pitaevskii mean field approach, Butts and Rokshar [21] and later Kavoulakis *et al.* [24] found geometric vortex configurations between distinct values of angular momentum [27, 28]. In analogy to mesoscopic superconducting disks, these vortex configurations again show selected symmetries corresponding to those of small Wigner crystallites [29].

Surprisingly, vortices may form independent of the statistics of the quantum particles. A striking identity between boson and fermion many-particle configurations leads to similar vortex states for bosons as well as for fermions, implying that vortex formation indeed is a universal phenomenon in a rotating quantum system [30].

At extreme angular momenta, far beyond the point where the vortex lattice melts [31], bosonic [32, 33, 34] as well as the fermionic *particles* crystallize [34, 35, 36], approaching the classical limit [37].

The purpose of this article is to show how *vortex formation and localization*, as well as the *crystallization of particles* at the limit of extreme rotation for bosons *and* fermions are connected. Our analysis is largely based on the fact that vortex formation can most easily be analyzed in terms of particle-hole duality, which was found to hold for the bosonic as well as the fermionic case [29].

This paper is organized as follows: In section II, after describing the model and methods, we briefly discuss the particle-hole dualism for the fermion vortex states. Results of the direct numerical diagonalization of the many-body Hamiltonian follow in III, where we discuss the localization for bosons and fermions at high angular momenta in terms of the regular oscillations in the yrast line. We apply similar arguments to explain the localization of vortices, both in the bosonic and fermionic limit. For fermions, this fact is further illustrated making use of particle-hole duality. Trial wave functions for the vortex states and the corresponding fermion-boson relations are discussed in section IV.

II. THE MODEL

A. The Hamiltonian

Let us now consider interacting particles confined by a two-dimensional harmonic trap. Ignoring the spin degree of freedom, these particles can either be spinless bosons (as for example, bosonic atoms in the same hyperfine state), or polarized spin-1/2 fermions (say, elec-

trons). The many-particle Hamiltonian is simply

$$H = -\frac{\hbar^2}{2\mu}\sum_i^N \Delta_i + \sum_i^N \frac{1}{2}\mu\omega^2 r_i^2 + \sum_{i<j}^N v(|\mathbf{r}_i - \mathbf{r}_j|) \quad (1)$$

where N is the number of particles with mass μ, ω the oscillation frequency of the confining potential, and $v(r)$ a *repulsive* two-body interaction. For a (dilute) gas of spinless, bosonic atoms, often a contact interaction of the form $v(r) = \frac{1}{2}U_0\delta(r)$ is used, where U_0 then depends on the scattering length for the atom-atom collisions [24]. For spinless fermions, however, this interaction only recovers the non-interacting case due to the Pauli principle. To ease the direct comparison between the boson and fermion spectra, in both cases we thus consider the usual long-range Coulomb form, $v(r) = e^2/4\pi\epsilon_o r$. For angular momenta well below the fractional quantum Hall regime [20, 25, 38], the boson spectra, calculated with either the short-range or long-range Coulomb interaction, in fact show a remarkable similarity, as earlier demonstrated by Toreblad *et al.* [30]. We refer to the work by Hussein *et al.* [39, 40, 41] and Vorov *et al.* [27] for a more general discussion of the universality of repulsive interactions in the bosonic case.

In what follows, we are mainly interested in the general structure of the eigenstates of Eq. 1 at high angular momentum M. We follow the nuclear physics tradition to study the so-called *yrast line*, i.e. the lowest-energy states as a function of M, and the corresponding low-lying excitations (the so-called *yrast spectrum* [42, 43]). Similarly, magnetic fields are not included explicitly: neglecting the Zeeman term, the only effect a magnetic field has, is to set the system rotating.

B. Restriction to the Lowest Landau Level

In the absence of interactions, the single-particle energies of the two-dimensional harmonic oscillator are $\epsilon = \hbar\omega(2n + |m| + 1)$, where n is the radial quantum number, and m the single-particle angular momentum. The energy level structure is schematically sketched in Figure 1. At very large total angular momentum of the non-interacting many-particle system, the lowest-energy state is characterized by quantum numbers $n = 0$, and m being zero or having the same sign as the total angular momentum, M. Measured relative to the non-interacting ground state, the total energy of the lowest state at a given M thus equals $\hbar\omega(M+1)$. This single-particle basis is identical to the so-called Lowest Landau Level (LLL) at strong magnetic fields. In this subspace, a configuration can be denoted by the Fock state $|n_0 n_1 n_2 \cdots n_s\rangle$, where n_i is the occupation number for the single-particle state with angular momentum i, and s the largest single-particle angular momentum included in the basis. For spinless fermions, n_i is 0 or 1 and for bosons it is an integer. As the angular momentum M is a good quantum number, we have the restriction $\sum_i i n_i = M$.

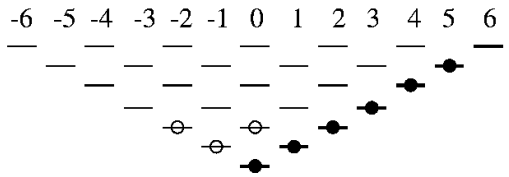

FIG. 1: Single-particle energy levels of a two-dimensional harmonic oscillator. The black bullets show the Maximum Density Droplet (MMD) configuration for six particles, and the open circles the $M = 0$ ground state for noninteracting, polarized fermions. The lowest-energy levels for each m form the Lowest Landau Level (LLL), as indicated by the bold lines.

For fermions, the smallest angular momentum that can be built in the LLL is that of the so called Maximum Density Droplet [44], $M_{MDD} = N(N-1)/2$, where due to the Pauli principle the lowest-energy states with successive single-particle angular momenta are occupied, generating a compact configuration

$$|\underbrace{111\ldots111}_{N}000\ldots\rangle \quad (2)$$

(see Fig. 1).

To see the similarity with quantum Hall systems [45], one may define a *filling factor* ν by the ratio between M_{MDD} and the actual angular momentum M,

$$\nu = N(N-1)/(2M)\ . \quad (3)$$

Clearly, the MDD corresponds to the Laughlin quantum Hall state at filling factor one in the bulk [46]. For bosons, the state with smallest possible angular momentum within the LLL is the *non-rotating* ground state, where all particles occupy the single quantum state with $n = 0$ and $m = 0$, i.e., $|\,N000\ldots\rangle$.

C. Numerical diagonalization of the Hamiltonian

Including now the interactions between the particles, we solve the full many-particle Hamiltonian exactly by numerical diagonalization, in order to obtain the ground state and the low-lying excited states at a given angular momentum M. In this so-called configuration interaction (CI) method, the many-particle state is described as a linear combination of Slater determinants, $|\Psi\rangle = \sum C_\alpha |\mathcal{L}_\alpha\rangle$, which for given statistics are defined by the combinatorics of the single-particle basis. Here, it is natural to use the basis of the Harmonic oscillator (i.e. that of the external trap). If the strength of the interparticle interaction is much smaller than the single-particle excitation energy $\hbar\omega$, at large M the most important configurations indeed consist of single-particle states of the LLL. In the limit $e^2/4\pi\epsilon_0 r_s \hbar\omega_0 \to 0$ (or $v_0/\hbar\omega_0 \to 0$), where r_s is the electron density parameter, $n_0 = 1/\pi r_s^2$, configurations with particles at higher Landau levels have

diminished weight C_α, and the LLL approaches the exact result. (For a discussion that includes Landau level mixing in the small-N limit, see the recent work by Stopa *et al.* [47], as well as Güçlü *et al.* [48, 49], considering quantum dots at high magnetic fields. A similar study was carried out for trapped bosons with contact interactions by Morris and Feder [50]).

Increasing the angular momentum beyond the MDD in the fermionic case, $M > M_{MDD}$, or beyond the "condensate", $M > 0$, in the bosonic case, there are many ways to distribute M quanta of angular momentum on the given number of particles, N. For large values of N and M, we thus have to restrict the basis by setting a smaller value s for the largest single-particle angular momentum. However, the most dominant configurations appear rather compact, i.e. most of the occupied single-particle states are close in angular momentum m. Thus, accurate results can still be obtained in a restricted Hilbert space.

In the LLL the single-particle basis states in polar coordinates (r, ϕ) are

$$\psi_m(r, \phi) = A_m r^m e^{-r^2/4} e^{im\phi}, \tag{4}$$

where A_m is a normalization factor.

The many-particle Hamiltonian, Eq. (1), can be written, apart from a constant, as

$$H = \sum_i m_i \hbar\omega c_i^+ c_i + \sum_{i,j,k,l} V_{ijkl} c_i^+ c_j^+ c_k c_l, \tag{5}$$

where

$$V_{ijkl} = \int\int d\mathbf{r} d\mathbf{r}' v(|\mathbf{r} - \mathbf{r}'|) \psi_i^*(\mathbf{r}) \psi_j^*(\mathbf{r}') \psi_k(\mathbf{r}) \psi_l(\mathbf{r}'), \tag{6}$$

and v is the interparticle interaction (see above). Since the total angular momentum is fixed, $M = \sum m_i$, the diagonal part gives an energy $\hbar\omega M$ for all configurations. In effect, we thus only diagonalize the interaction part of the Hamiltonian. This simplification is caused by the restriction of the basis to the lowest Landau level and holds for bosons as well as for fermions. It is natural to present the energies of the interaction part only (which trivially scales with its strength), as done for most of the results shown below.

The interaction matrix elements are computed numerically. In the case of Coulomb interaction we used the technique suggested by Stone *et al.* [51]. For numerical diagonalization of the Hamiltonian matrix, we applied the Lanczos method [52].

D. Particle-hole duality

A Fock state can be described either by particles, or equivalently, by holes. For spinless fermions, in practice one simply can replace the zeros with ones, and vice versa the ones with zeros. For example, the configuration $|1110011111\rangle$ is then changed to $|0001100000\rangle$. One correspondingly defines the creation (annihilation) operator of a hole as $d^+ = c$ ($d = c^+$) and writes the Hamiltonian Eq. (5) in terms of these:

$$\begin{aligned} H &= \sum_i m_i \hbar\omega_0 (1 - d_i^+ d_i) + 2 \sum_{i,j} (V_{ijij} - V_{ijji}) d_i^+ d_i \\ &+ \sum_{i,j,k,l} V_{ijkl} d_l^+ d_k^+ d_j d_i + \text{constant}. \end{aligned} \tag{7}$$

Naturally, the solution of this Hamiltonian leads to an equivalent result, and requires the same numerical effort.

The interactions between the holes here are the same as the interactions between the particles. However, it is important to note that the second term is nonzero. This means that the holes effectively do not move in a harmonic confinement. This has two important consequences: the holes (*i*) do not have a pure center of mass excitation, and (*ii*) not necessarily the same localization geometry as the particles.

This particle-hole dualism, as earlier described in Ref. [29], allows us to identify the holes as vortices in the Fermi sea and to evaluate the correlation functions between these vortices. Furthermore, in the case of a few holes in the Fermi sea, the energy spectrum is dominated by these holes and can be understood by diagonalizing only the interaction part of the hole Hamiltonian (i.e. the third term in Eq. (7)).

III. RESULTS

A. Localization of particles at extreme angular momenta

Let us first analyze the many-body quantum spectra for small particle numbers. (This will later turn useful when studying the spectral properties of many-particle systems in terms of localized vortices).

Figure 2 compares the spectra for three bosons (*red crosses*, +) and three fermions (*blue crosses*, ×) at extreme angular momenta, $M > 3M_{MDD}$. (Only the nontrivial interaction part of the total energy is shown, here for the ten lowest states at fixed M). Naturally, the interaction energy goes down with increasing angular momentum for repulsive interactions. Note that for each new energy at a given value M', the same energy is reproduced at all angular momenta $M > M'$. These are simply the center of mass excitations characteristic for harmonic confinement [53]. With increasing M, the boson and fermion spectra become remarkably similar. This does not only hold for the yrast line, but also for the low-lying excitations.

The yrast line (drawn in Fig. 2 as a red line to guide the eye) shows clear oscillations with a period of $\Delta M = 3$. The inset shows the corresponding spectrum for $N = 2$, with a similar oscillation in the yrast states, alternating between even and odd angular momenta, respectively. Further increasing the number of particles, we show in Fig. 3 the yrast spectrum for $N = 6$ bosons. Again, the

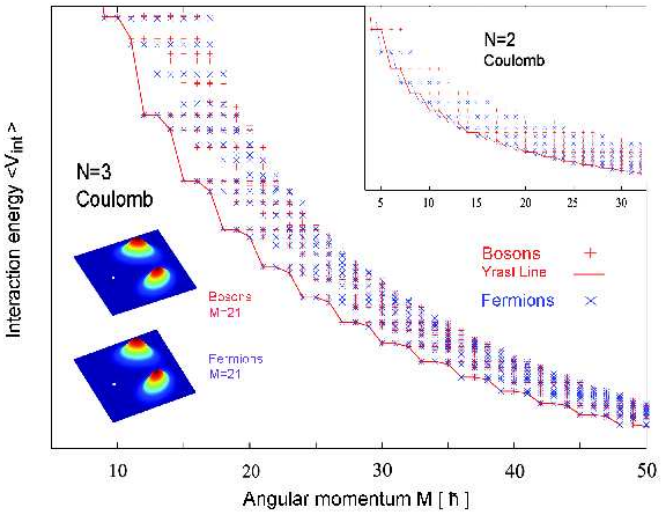

FIG. 2: Interaction energy of a three-particle system, $N = 3$, for bosons (*red crosses,* $+$) and fermions (*blue crosses*, $\times$), as a function of the angular momentum, for angular momenta $M > 3M_{MDD}$. (The inset to the right shows the same for $N = 2$). The red (blue) line is the yrast line. The insets to the left show the boson and fermion correlation functions, here taken at the cusp states with $M = 21$ as an example. The white dot indicates the reference point. The particles appear localized at the corners of a triangle, with one particle placed at the reference point.

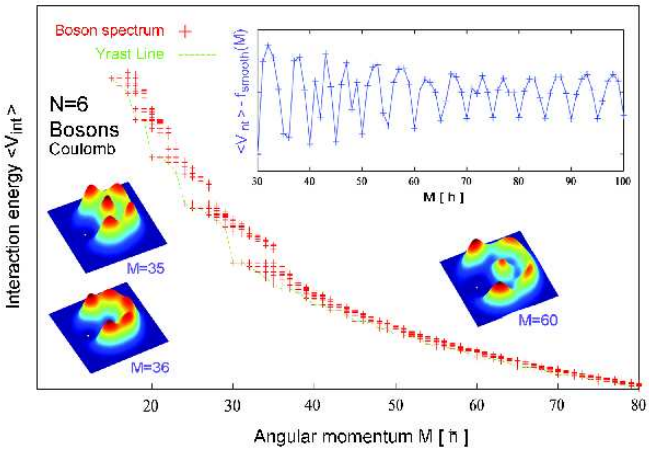

FIG. 3: Interaction energy of $N = 6$ bosons as a function of the angular momentum. The inset shows the yrast line with a smooth function of angular momentum (3rd order polynomial) subtracted from the energies, in order to make the oscillations more visible. The large-M limit is dominated by a regular oscillation with $\Delta M = 5$. The pair correlation functions to the left clearly demonstrate localization in Wigner molecule geometries at high angular momenta. While at smaller M-values, the $(1, 5)$ and the $(0, 6)$ configurations compete, at extreme angular momenta fivefold symmetry dominates.

boson and fermion spectra (not plotted here) are very similar in the large-M limit.

Similar to the results shown for $N = 3$ in Fig. 2 above, the boson spectrum in Fig. 3 shows pronounced cusps with a characteristic gap to the low-lying excitations. At smaller M, oscillation periods with $\Delta M = 5$ and $\Delta M = 6$ compete, with cusps at $M = 18, 20, 24, 25, 30, 36, 40....$ Beyond $M = 50$ the cusps appear regularly with $\Delta M = 6$. This is very clearly seen in the inset to Fig. 3, where a third order polynomial in M was subtracted from the energies, changing the slope of the yrast line in order to make its oscillations more visible.

These cusp states and their periodicities in M are a phenomenon well known to occur in quantum dots at very strong magnetic fields, which have been investigated extensively in the literature [45]. Here, the regular oscillations of ground state energy as a function of magnetic field were found to originate from rigid rotations of the classical electron configurations [54, 55]. While for particle numbers up to $N = 5$, the Wigner crystallites form simple polygons (from triangle to pentagon), the case $N = 6$ is more complicated due to the interplay between two stable classical geometries, a pentagon with one particle at the center, $(1, 5)$, and a hexagon, $(0, 6)$ [32].

These simple geometries in fact easily explain the periodic oscillations in the above many-body spectra. The rigid rotation of the 'molecule' of localized particles is only possible at angular momenta allowed by the underlying symmetry group [34]. For example, if the electrons localize for example in an equilateral triangle, the threefold symmetry leads to period of three. The five-fold symmetry of the $(1, 5)$ ground state of the six-electron molecule yields a period of five [32, 45, 56, 57]. Correspondingly, the period $\Delta M = 6$ is explained by the hexagonal structure, $(0, 6)$.

A related periodicity of the yrast energy as a function of the angular momentum is obtained also for other particle numbers, and holds even if higher Landau levels are included in the basis set [32, 54, 55, 58]. (Similar agruments were successfully applied earlier also to analyze the rotational spectrum of quasi-one-dimensional quantum rings, see [56, 57]).

The particle localization in the internal coordinates of the quantum system can be demonstrated further by using a rotating frame [55], or by studying the pair correlations defined as

$$g(\mathbf{r}, \mathbf{r}') = \langle \Psi | \hat{n}(\mathbf{r}) \hat{n}(\mathbf{r}') | \Psi \rangle \ , \qquad (8)$$

where $\hat{n}$ is the density operator. The pair correlation function g describes the probability to find a particle at $\mathbf{r}'$ when another particle is in the reference point $\mathbf{r}$. In a finite system, the pair correlation function is a function of two variables, and often also called "conditional probability". In Fig. 2 (*left*) we show the pair correlations for the three-particle system, both in the bosonic and fermionic case, at $M = 21$. In both cases, the particles appear localized in a triangular geometry, with two particles showing clear maxima opposite to the reference

point (indicated by the white dot). A very similar result is obtained for the six-particle system, where at smaller M-values, the $(1,5)$ and the $(0,6)$ configurations compete. At extreme angular momenta, however, as here shown for $M = 60$, the fivefold symmetry $(1,5)$ dominates. These pair correlations clearly demonstrate that at high angular momenta, bosons as well as fermions localize in Wigner molecule geometries, in excellent agreement with the earlier results by Manninen *et al.* [32], and their subsequent confirmation by Romanovsky *et al.* [33].

B. Localization of Vortices

For a harmonically trapped cloud of bosons that is set moderately rotating, geometric vortex configurations are known to appear between distinct values of angular momentum. A single vortex at the center of the system is formed when $M = N$, two vortices at about $M = 1.7N$, three vortices when $M = 2.1N$ and N vortices before $M = 3N$. It was shown earlier that these mean-field results within the Gross-Pitaevskii scheme [21, 24] emerge as the correct leading order approximation to exact calculations in the same subspace [59].

The many-body spectra for 20 and 40 bosons interacting by the Coulomb force, are compared in Figure 4, displaying the yrast line and up to ten low-lying excitations. The horizontal axis is now the angular momentum per particle, $l = M/N$. As previously, a second-order polynomial in M was subtracted to emphasize the salient oscillations of the yrast line. For these large particle numbers, the Hilbert space was truncated such that only single-particle states with $m \leq 10$ were included, still giving well-converged results in the bosonic case.

Both spectra show pronounced oscillations with consecutive periods of $\Delta M = 2, 3$ and 4, expanding through the above mentioned intervals of subsequent vortex entry. While a single vortex is formed at $l = 1$, oscillations with $\Delta M = 2$ coincide with the two-vortex solution appearing between $1.7 < l < 2.1$, three vortices beyond $l = 2.1$, etc. These results are in excellent agreement with the results of the Gross-Pitaevskii approximation [24].

The regular oscillations in fact appear very similar to the cusp states at extreme angular momentum, as discussed for small particle numbers in Figs. 2 and 3 above. However, in contrast to localization in Wigner molecules, these oscillation are now caused by two, three, or four localized *vortices*, respectively. (The 2- and 3-vortex geometries are schematically sketched in Figs. 4 and 5 below).

We notice that the spectra look qualitatively very similar to that for 20 fermions shown in Fig. 5. There is, however, a marked quantitative difference in the angular momentum where the vortices appear. In the case of bosons, the value of angular momentum per particle M/N where the second, third, etc. vortex enters the cloud, seems to be independent of the number of bosons in the system. (Naturally the number of particles has to

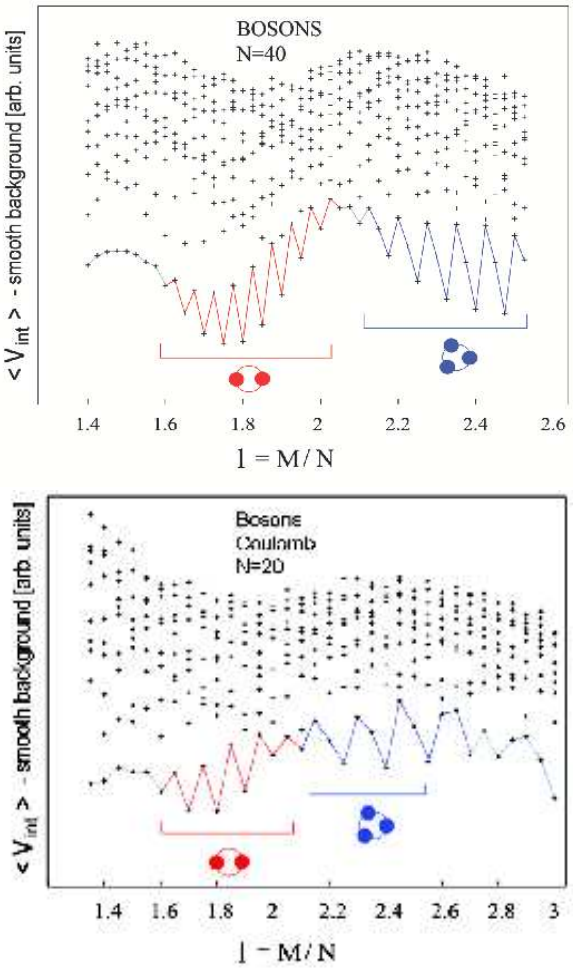

FIG. 4: Many-particle energy levels for 20 (*lower panel*) and 40 bosons (*upper panel*) as a function of angular momentum per particle, $l = L/M$. In both cases, a second-order polynomial in M was subtracted from the energies to make the yrast line nearly horizontal.

be much larger than the number of vortices). If the same systematics would hold for fermions, we should expect the same small number of vortices to appear when the angular momentum is increased beyond the MDD. This, however, does not hold for $N \geq 12$. The vortex systematics then changes [60, 61, 62] as compared to the bosonic case. The increase of angular momentum per particle, $(M - M_{MDD})/N$, for the appearance of the second vortex depends on N, as illustrated in Table I.

The origin of the periodic oscillations can be understood by studying the corresponding many-particle problem of holes, as briefly discussed in section II D above.

For this purpose, let us now study in more detail the fermion case. The excitations from the MDD to higher angular momenta create holes in the filled Fermi sea. These holes are associated with the existence of vortices in the system [29]. In the single-vortex region, the most important configuration has a single hole at angu-

TABLE I: Angular momenta where the vortices appear for boson and fermion systems of different sizes. N is the number of particles, M the angular momentum and $\bar{M} = M - M_{MDD}$

	$[M/N]$ for bosons			$[\bar{M}/N]$ for fermions	
vortex	$N=8$	$N=20$	$N=40$	$N=8$	$N=20$
2nd	1.7	1.6	1.6	1.7	0.9
3rd	2.2	2.1	2.1	2.2	1.4
4th		2.8	2.8		2.2

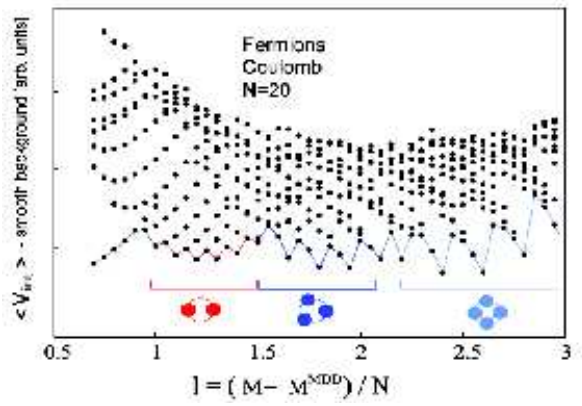

FIG. 5: Many-particle energy levels for 20 fermions as a function of angular momentum per particle relative to the MDD, $l = (M - M_{MDD})/N$. As in Fig. 4 above, a second-order polyonomial was subtracted from the yrast line.

lar momentum $M_h = M_{\rm MDD} + N - M$. When M is increased from the MDD the single vortex enters the system from the surface and reaches the center at angular momentum $M = M_{\rm MDD} + N$. Then, $M_h = 0$, i.e. the Fock state with the largest amplitude has the structure $|\,0111\ldots1111111000\ldots\rangle$. This state appears in the excitation spectrum and terminates the band [61]: Within the lowest Landau level, no further quanta of angular momentum can be added, unless a second hole penetrates the electron droplet. Note that the single hole has a simple single-particle wave function, as in Eq. (4), i.e. the hole (or vortex) is either localized at the center, or delocalized on a ring.

The single vortex does not reach the origin before it is energetically more favorable to create two vortices that are closer to the surface. Considering the state for holes, the angular momentum is written as

$$M_h = \frac{(N+h)(N+h-1)}{2} - M, \qquad (9)$$

where h is the number of holes and M the angular momentum of the fermion system. For example, the 20-particle state with angular momentum $M = M_{MDD} + 24 = 214$ corresponds to a two-hole state with $M_h = 17$. The two-hole state at such high angular momentum is strongly correlated, with holes localizing in a narrow ring, as shown in Fig. 6 below.

Similar to the particle-particle (pp) correlations, we can define a hole-hole (hh) correlation function

$$g_{hh}(\mathbf{r},\mathbf{r}') = \langle\Psi|\hat{h}(\mathbf{r})\hat{h}(\mathbf{r}')|\Psi\rangle, \qquad (10)$$

where $\hat{h}(\mathbf{r}) = \sum_{i,j}\psi_i^*(\mathbf{r})\psi_j(\mathbf{r})d_i^+ d_j$ is the hole density operator.

The pair correlation between the holes clearly shows that in the internal frame, the holes indeed are localized. Fig. 6 shows the that the density profile of the two holes forms a narrow ring. At the same radius, the hh-correlation shows a very well localized maximum, corresponding to a hole (vortex) localized at the opposite side of the "reference hole".

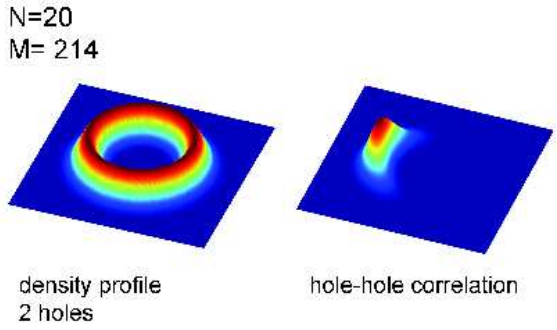

FIG. 6: Density profile of two holes at angular momentum $M_h = 17$ (a) and the corresponding hole-hole correlations (b). The hole density and pair correlation was determined from the calculation for 20 electrons with angular momentum $M = 214$ and the minimum single-particle basis allowing that angular momentum.

Considering the two-hole system as a rigid "molecule" of two vortices, the oscillations in the energy spectrum consequently are understood as resulting from the rotational states: Like for a two-atomic molecule, only every second angular momentum is allowed in the rotational spectrum [63]. At angular momenta in between, the rotational state must be occupied by a vibrational excitation. Thus, the state has higher energy. Similarly, this holds for the periodic oscillations of the two-particle yrast line for bosons as well as fermions, as displayed in the inset to Fig. 2 above.

Increasing the angular momentum, the whole system expands, while the vortices move closer to the center. Beyond a certain angular momentum, however, the repulsion between the vortices becomes so strong that it is energetically favorable to form a larger ring with three vortices instead. In this region, the spectrum (Fig. 5) then shows an oscillation period with $\Delta M = 3$, caused by the rigid rotation of the triangle of *three* vortices. Further increasing the angular momentum adds additional vortices, with the oscillation period increased by one each time a new vortex enters the system.

Let us now study in more detail the three-vortex region, and compare the spectrum calculated for only three

fermions, as shown in Fig. 2, with that for 20 fermions, as displayed in the lower panel of Fig. 7. (For a quantitative comparison of the spectra, we first subtracted from the 20-fermion spectrum a linear function $0.9M$ and then plot it as a function of the corresponding hole angular momentum as defined in Eq. (9)).

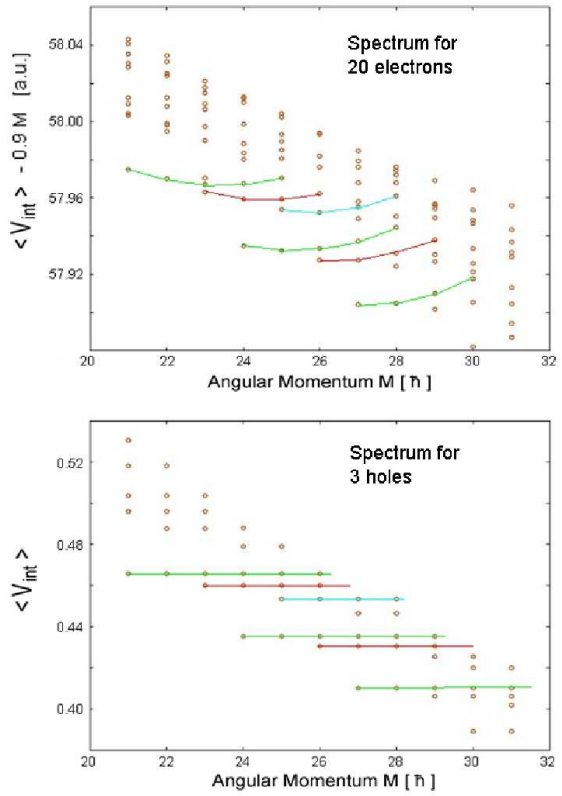

FIG. 7: (a) Many-particle spectrum for three holes, as determined from the 20-fermion spectrum (see text). A linear function $0.9M$ was subtracted. The hole spectrum compares well with that of three *particles*, shown in (b) for Coulomb interactions. The horizontal lines in (b) connect states which are center-of-mass excitations. To guide the eye, corresponding lines are plotted in (a).

The spectra are strikingly similar, indicating that indeed the spectrum of 20 particles (in this region) is determined by the three localized holes. The lines in Fig. 7 indicate the center of mass excitations for three particles. In the 20-particle spectrum, these states are not pure center of mass excitations of holes, since the true Hamiltonian for holes, Eq. (7), has additional terms with anharmonic corrections to the confining potential.

The observation that these quantum states show much similarity in their internal structure is further clarified by comparing their pair correlations. Fig. 8 shows the *pp* correlations at three points along the yrast line. When the yrast line has a kink, as here for example at $M_h = 15$ or $M = 239$, the correlation function clearly shows localization of holes in a triangular geometry. At $M_h = 16$ the three-particle system originated from the $M_h = 15$ state by a center of mass excitation, and at $M_h = 17$ it has an internal vibrational mode [34, 37]. The effect of these excitations is clearly seen in the correlation functions. The correspondence between *hh* and *pp* correlations for $N = 3$ and $N = 20$, is not perfect, however, since in the 20-particle system the center of mass excitation (for holes) is mixed with the vibrational excitation.

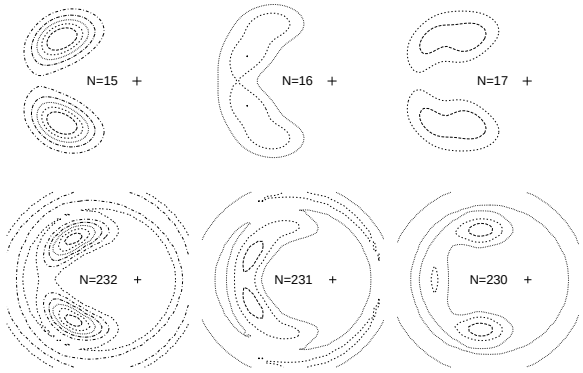

FIG. 8: The *lower panel* shows contours of the *hh*-correlations for three-vortex states of a 20-fermion system (Coulomb) at angular momenta $M = 230$, $M = 231$ and $M = 232$. The *upper panel* shows the corresponding *pp*-correlations for *three* particles, at $M = 15$, 16 and 17.

The three-particle and the three-hole states for $N = 20$ can be compared directly by calculating their overlaps. In doing so, the electron calculation has to be restricted to the minimum Hilbert space having only three holes. As an example, we calculated the overlap matrix for the four lowest energy states at angular momentum $M = 24$ for the holes (the corresponding 20 electron angular momentum is 229). The result is shown in Fig. 9. The overlap between the ground states of the two calculations is large, showing again that their internal structure is similar. The first and second excited states seem to be mixed, while the third excited state is again quite similar. This result is in agreement with the pair correlation functions (Fig. 8) and the spectra (Fig. 7) which show that a pure center of mass excitation of holes (first excited state here) does not exist in the 20-particle spectrum.

For small particle numbers, $N \lesssim 10$, the pair correlations cannot display the vortex structure properly. In this case, weak signals of vortices can be seen only if the reference point is clearly outside the density distribution [64], since then the exchange-correlation hole is distributed rather evenly over the remaining dot area.

The situation becomes different, when the particle number is significantly increased. Figure 10 shows the electron-electron pair correlation for 36 electrons. In the MDD, only the exchange hole at the reference point is clearly visible. In the case of $M = 706$, in addition to the exchange hole we see four wide minima, which we interprete as four localized vortices. The reference point is chosen at a radius where the density has a mini-

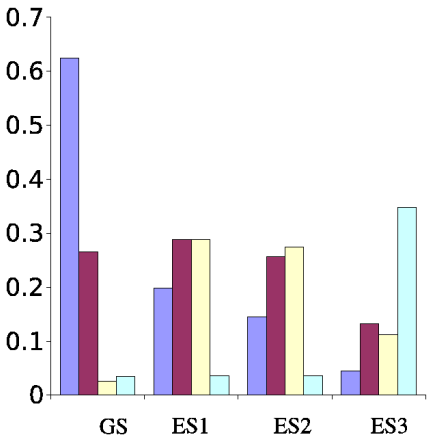

FIG. 9: Overlaps between 3-hole states from two different calculations for $M_h = 24$ ($M = 22$). GS, ES1, ES2 and ES3 refer to the ground state, and excited states of the three particle calculation. The columns show the overlaps with the ground state (blue), and the first three excited states (red, yellow and green) of the hole state derived from the 20 electron-calculation.

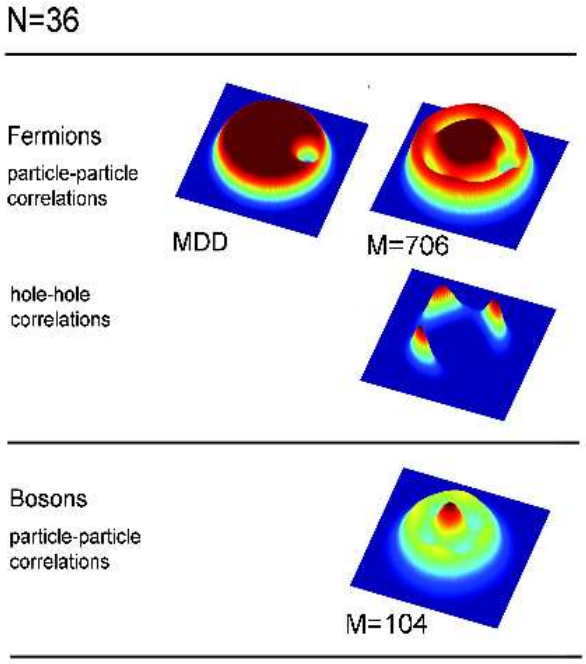

FIG. 10: Pair correlation functions calculated for 36 electrons. The *upper panel* shows the electron-electron correlations for the MMD (*left*), for particles at $M = 706$ showing four vortices (*right*), and for holes at the same angular momentum (*lower right*). The *lower panel* shows the corresponding correlation function for a bosonic four-vortex state at angular momentum $M = 104$. (Note the absence of the exchange hole in the bosonic case.)

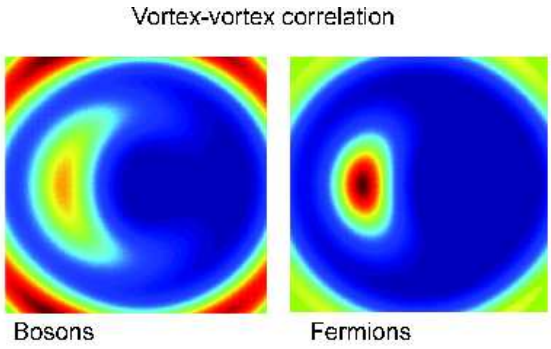

FIG. 11: Vortex-vortex correlation function of the two-vortex state for 20 bosons with $M = 34$, $M/N = 1.7$, left, and for 20 fermions with $M = M_{MDD} + 34 = 224$. The fermion state is the second excited state for that angular momentum. For bosons the correlation function is determined by transforming the boson state to a fermions state and plotting the hole-hole correlation.

mum, i.e. at the expected radius of the vortex ring. The *hh*-correlation, also shown in Fig. 10, shows three pronounced maxima, which are consistent with the minima in the *pp*-correlation. This comparison demonstrates, that the vortex localization is more clearly seen in the *hh*-correlations, than in the *ee*-correlations. The lowest panel in Fig. 10 shows the corresponding pair correlations in the bosonic case. Also in this case, we see four minima, corresponding to the four vortices, but naturally, not the exchange hole.

Regarding the analysis of the corresponding Fock states in the bosonic case, it is not as straightforward to relate the vortices to holes in the similar fashion as for spinless fermions. Nevertheless, we can transform the boson wave function to a fermion wave function using the method explained in Ref. [30] and then plot the vortex-vortex correlation for the corresponding fermion system. Figure 11 shows a pair correlation function constructed in this way, with the localization of the second vortex opposite to the reference point.

C. Comparison between boson and fermion wave functions

Comparing the energy spectra and the pair correlation functions, the vortex formation for bosons and fermions appears surprisingly similar. It is now interesting to see how far this similarity is reflected in the detailed structure of the many-particle states. For this purpose, we need to compare the fermion wave function with angular momentum $M - M_{MDD}$ to the boson wave function with M. To this end, we should multiply the boson wave function with the determinant $\prod(z_i - z_j)$. Here, we instead use a simpler mapping based on the one-to-one correspondence between the boson and fermion configurations, as described earlier by Toreblad *et al.* [30]. The bose "condensate", $|N0000\cdots\rangle$, corresponds to the MDD in the fermion case. Other configurations can be obtained as single-particle excitations out of the condensate. Ta-

ble II shows a few examples of these configurations, here for the simple case of six particles. Figure 12 compares

TABLE II: Examples of corresponding configurations for six fermions and bosons. M is the angular momentum of the configuration. For six fermions the angular momentum of the MDD is 15.

M_{fermion}	fermion state	M_{boson}	boson state
15+0	$\|1111110000\rangle$	0	$\|600000\rangle$
15+4	$\|1101111000\rangle$	4	$\|240000\rangle$
15+4	$\|1111001100\rangle$	4	$\|402000\rangle$
15+15	$\|1000111110\rangle$	0	$\|100500\rangle$

the amplitudes of the most important configurations for the two-vortex state of 20 bosons with $M = 34$ to those of 20 fermions with $M = 224$. For bosons, the state is at the yrast line, while for fermions it is the second excited state. The yellow columns show the cumulative overlap between the boson and fermion states. The configurations are shown at the right, using the notation for bosons. The figure shows that for both kinds of particles, the same configurations are important. The actual amplitudes differ, but the qualitative similarity of the states is clearly seen, especially regarding the signs of the different terms contributing to the linear combination of Slater determinants in the many-body state.

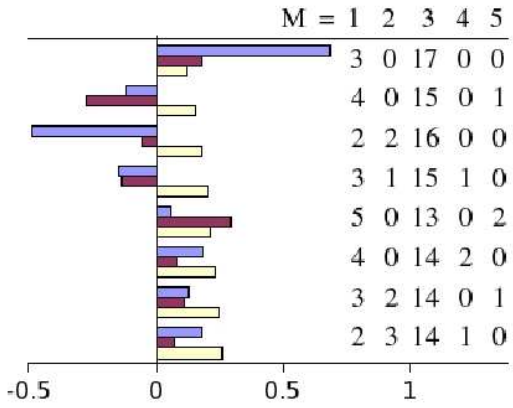

FIG. 12: Comparison of the coefficients of the most important configurations of the two-vortex state of 20 bosons with $M = 34$ to those of 20 fermions with $M = 224$. In the case of fermions the state is the second excited state for the chosen angular momentum. For fermions, the amplitudes are shown in blue, and for bosons in red. The yellow columns show the cumulative overlap between the boson and fermion states. The configurations are shown at the right, using the notation for bosons.

D. Density and vorticity

Any exact solution of interacting particles in circularly symmetric potential must have a density with circular symmetry. Thus, only the radial density distribution is relevant. In the LLL the density can be simply determined from the occupancies of the single-particle levels

$$n(r) = \sum_\alpha |C_\alpha|^2 \sum_m n_{\alpha m} |\psi_m(r,\theta)|^2, \tag{11}$$

where C_α is the amplitude of the configuration α, $n_{\alpha m}$ the occupation number of the single particle state m in configuration α, and ψ_m the single-particle state of Eq. (4). We note that the same information is contained in the occupancy of the single-particle angular momentum states:

$$D(m) = \sum_\alpha |C_\alpha|^2 n_{\alpha m}. \tag{12}$$

The restriction to the LLL makes it simple to determine the current density

$$j_\theta(r) = \sum_\alpha |C_\alpha|^2 \sum_m n_{\alpha m} \frac{m}{r} |\psi_m(r,\theta)|^2, \tag{13}$$

and the velocity field $j_\theta(r)/n(r)$. Naturally, the current density as well as the velocity field have the circular symmetry of the underlying Hamiltonian.

We can also use the vorticity of the velocity field

$$\nabla \times \left(\frac{j_\theta(r)}{n(r)} \right) \mathbf{e}_\theta = \frac{\partial}{\partial r} \left(\frac{j_\theta(r)}{n(r)} \right) \mathbf{e}_z \tag{14}$$

to give information about the vortex formation. If the vortex is at the center of the trap, naturally the density of the single-vortex state is rotationally invariant. However, if one or more vortices are off-center, their characterization is not as straight-forward.

For example, the two-vortex solution, as displayed in Fig. 13, shows a clear maximum in vorticity where the radial density profile has a local minimum. The profiles of the density and vorticity for bosons and fermions, respectively, appear rather similar, with the main difference that the fermionic cloud extends to larger radius as a simple consequence of the Pauli principle.

IV. TRIAL WAVE FUNCTIONS FOR VORTEX STATES AND FERMION-BOSON RELATIONS

The fermion wave function for the maximum density droplet (MDD) is a single determinant, see Eq. (2), where the number of singly occupied states equals the number of particles. Using the single-particle states of the LLL, Eq. (4), now in terms of the complex coordinates $z_j = x_j + iy_j$, this takes the form of the Laughlin wave function [46] which, apart from the normalization, is written as

$$\Psi_q^F = \prod_{i<j}^N (z_i - z_j)^q \exp\left(-\sum_k |z_k|^2/4 \right), \tag{15}$$

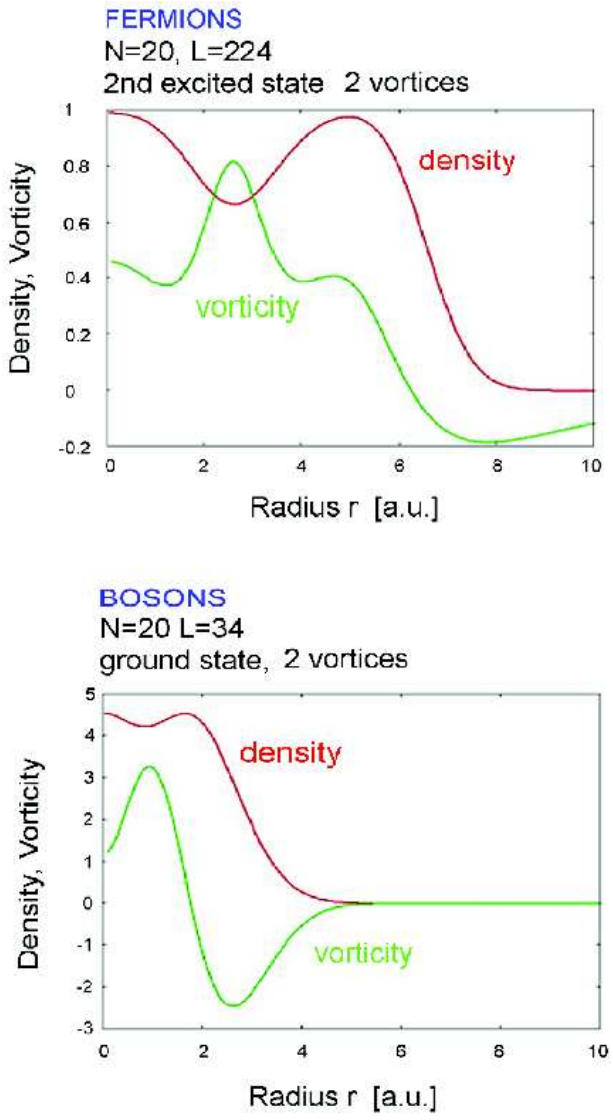

FIG. 13: Density (*red lines*) and vorticity (*green lines*) in a fermionic (*upper panel*) and bosonic (*lower panel*) system, respectively. For $N = 20$ particles, the fermionic two-vortex state at $M = 190 + 34$ is compared to its bosonic counterpart at $M = 34$.

where $q = 1$ for MDD and in general an odd integer for fermions. For the MDD, we use the notation $\Psi_1^F = \Psi_{MDD}^F$. When the angular momentum is increased, there is no simple analytic formula for the exact state. However, it has been shown that at $3M_{MDD}$, the next Laughlin state with $q = 3$ corresponding to the filling factor $\nu = 1/3$ for the fractional quantum Hall effect is a good *approximation* to the exact wave function [32]. For angular momenta in between the Laughlin states, no simple analytic expressions for the wave function exist.

Rather than providing accurate analytic estimates for the many-body wave function, our aim here only is to reach a physical understanding of vortex formation and crystallization at high angular momenta. To this end, let us first consider the simplest case of a single vortex. Bertsch and Papenbrock [23] have shown that for weakly interacting bosons, a single vortex at the center of the condensate can be described as

$$\Psi_{1v}^B = \prod_i^N (z_i - z_0) \exp\left(-\sum_k |z_k|^2/4\right), \qquad (16)$$

where $z_0 = (z_1 + z_2 + \cdots z_N)/N$ is the center-of-mass coordinate. We can use the same Ansatz for fermions and write [32]

$$\Psi_{1v}^F = \prod_i^N (z_i - z_0)\Psi_{MDD}^F. \qquad (17)$$

Note that the only difference between the boson and fermion states is the additional product $\prod_{i<j}^N (z_i - z_j)$ which makes the fermion state antisymmetric. We have tested this approximation in the case of six electrons. In this case, the overlap between the trial wave function Eq. (17) and the exact result (restricted to LLL) for Coulomb interaction is 98.5 %. Even when the restriction to LLL is abandoned and higher Landau levels are included, the overlap was found [32] to be 90% .

The most important configuration of the Bertsch-Papenbrock state Eq. (16) for, say six, fermions is $|01111110000\rangle$, i.e. one electron is removed from the angular momentum $m = 0$ state and lifted to the first empty angular momentum state. We notice that this is the smallest angular momentum state that can have an empty state at $m = 0$. For six electrons, $M_{MDD} + N = 15 + 6 = 21$. For smaller values of M the empty state is at a higher single-particle state. For example, for $M = M_{MDD} + 1$ the only possible configuration is $|11111010000\rangle$ and the corresponding wave function is $x_0\Psi_{MDD}^F$. When the angular momentum is increased, the hole in the Fermi sea moves to lower angular momentum until it reaches the origin. We will call these states as one-vortex states. When the hole is not at $m = 0$ the vortex is not localized at the origin, but de-localized in a ring at a radius which depends on the angular momentum of the hole.

In the case of many vortices, simple analytic approximations for the states are not known. However, we can guess the most important configuration with the help of the following arguments [30]. First we notice that for a large number of particles we can replace the center of mass in Eq. (16) with the origin, i.e. with a fixed point. In the same spirit we can assume several localized vortices at fixed points. When the number of vortices is small, their geometrical arrangement will be on a ring. In this case the wave function corresponding to Eq. (16) would be

$$\begin{aligned}\Psi_{kV} &= \prod_{j_1}^N (z_{j_1} - ae^{i\alpha_1}) \times \cdots \times \prod_{j_k}^N (z_{j_k} - ae^{i\alpha_k})\Psi_{MDD} \\ &= \prod_j^N (z_j^k - a^n)\Psi_{MDD}\ , \end{aligned} \qquad (18)$$

where k is the number of vortices, a is distance of the vortices from the origin and $\alpha_j = 2\pi j/k$. Clearly, the above wave function does not have a good angular momentum. Projecting to a good angular momentum means collecting out states with a given power of a. We get a state

$$\Psi_{kV} = a^{k(N-K)} \mathcal{S} \left(\prod_j^K z_j^k \right) \Psi_{MDD} \tag{19}$$

which now corresponds to a good angular momentum $M = M_{MDD} + kK$. Expanding the polynomial in Eq. (19) shows that the most important configuration has the form

$$|\underbrace{1111}_{N-K}000\underbrace{11111111110}_{K}0000000\rangle, \tag{20}$$

where the number of adjacent zeros between the one's equals the number of vortices, and the number of ones after the zeros equals to K.

In the case of bosons, a trial wave function can be constructed in a similar fashion, the only difference being that the MDD wave function, Eq. (15), is replaced by the Bose condensate, $\exp(-\sum |z_k|^2)$. This means that the trial wave functions for bosons and fermions are similar apart from the product in Eq. (15), which makes the fermionic state antisymmetric.

Though originally developed to describe fractional quantum Hall states, a tool that has shown useful to describe the high angular momentum states of rotating bose condensates [25, 38, 65, 66, 67, 68] is the composite fermion model of Jain [69]. In this method, the wave function for any M is determined first using also higher Landau levels and then projected to the lowest Landau level. While it would be expected to be applicable in the regime $M \sim N^2$, it was more recently extended successfully to describe angular momenta even before the unit vortex [65, 70].

The construction of the composite fermion state is complicated due to the projection to the LLL and does not easily reveal the nature of the solution. Nevertheless, the composite fermion picture shows that there is a relation between the states of the spinless fermions and bosons. In fact, it has been shown [71] that in the analytically solvable model of harmonic interparticle interactions, this relation between the bosonic and fermionic solutions is exact and the states can be written as a product of a symmetric homomorphic polynomial P_M and the boson or fermion condensate for fermions,

$$\Psi_{M_{MDD}+M} = P_M \prod (z_i - z_j) \exp\left(-\sum_k |z_k|^2/4 \right) \tag{21}$$

and for bosons,

$$\Psi_M = P_M \exp\left(-\sum_k |z_k|^2/4 \right) . \tag{22}$$

The only difference between the boson and fermion states is then the product that makes the fermion state antisymmetric. (In the case of the Laughlin state with $q \geq 3$ the symmetric polynomial is simply $P_{(q-1)N(N-1)/2} = \prod (z_i - z_j)^{q-1}$).

V. CONCLUSIONS

At extreme angular momenta, a few particles in a harmonic trap crystallize, indpendent of their fermionic or bosonic nature. In much analogy to what was observed in quantum dots at strong magnetic fields [54, 55], this crystallization is apparent from the regular oscillations in the quantum many-body spectrum: Cusps at the yrast line, and their periodicity in angular momentum, are easily understood in terms of the simple geometries of these so-called Wigner molecules, being of either fermionic or bosonic nature [32, 33].

At moderate angular momenta, however, it is known that vortices may form, independent of the system being bosonic or fermionic. In a harmonic confinement, these "holes" that are penetrating the rotating quantum system, arrange in simple polygonal structures, very similar to those of the localized Wigner crystallites of particles. They lead to similar cusp states in the yrast line, with oscillation periods simply following the underlying symmetry of the "vortex crystal". We showed how this mapping could be understood in terms of particle-hole duality, holding for the bosonic as well as the fermionic case [29].

Acknowledgements

We thank D. Pfannkuche, B. Mottelson, S. Viefers, J. Jain, H. Saarikoski and E. Räsänen for rewarding discussions. Financial support from the Swedish Foundation for Strategic Research and the Swedish Research Council, from NordForsk as well as the Academy of Finland is gratefully acknowledged.

[1] A.A. Abrikosov, Sov. Phys. JETP **5**, 1174 (1957); Phys. Chem. Solids **2**, 199 (1957).
[2] V.A. Schweigert, F.M. Peeters, and P. Singha Deo, Phys. Rev. Lett. **81**, 2783 (1998).
[3] B.J. Baelus, F.M. Peeters, and V.A. Schweigert, Phys. Rev. B **63**, 144517 (2001).
[4] B.J. Baelus and F.M. Peeters, Phys. Rev. B **65**, 104515 (2002).

[5] B.J. Baelus, L.R.E. Cabral, and F.M. Peeters, Phys. Rev. B **69**, 064506 (2004).

[6] F. Bolton and U. Rössler, Superlattices Microstruct. **13**, 139 (1993).

[7] V.M. Bedanov and F.M. Peeters, Phys. Rev. B **49**, 2667 (1994).

[8] I.V. Grigorieva, W. Escoffier, J. Richardson, L.Y. Vinnikov, S. Dubonos, and V. Oboznov, Phys. Rev. Lett. **96**, 077005 (2006).

[9] F. Dalfovo, S. Giorgini, L.P. Pitaevskii, and S. Stringari, Rev. Mod. Phys. **71**, 463 (1999).

[10] A.J. Leggett, Rev. Mod. Phys. 73, 307 (2001).

[11] C.J. Pethick, and H. Smith, *Bose-Einstein condensation in dilute gases.* (Cambridge University Press, Cambridge, 2002).

[12] K.W. Madison, F. Chevy, W. Wohlleben, J. Dalibard, Phys. Rev. Lett. **84**, 806 (2000).

[13] F. Chevy, K. Madison, and J. Dalibard, Phys. Rev. Lett. **85**, 2223 (2000).

[14] J.R. Abo-Shaer, C. Raman, J.M. Vogels, and W. Ketterle, Science **292**, 476 (2001).

[15] D.S. Rokshar, Phys. Rev. Lett. **79**, 2164 (1997).

[16] J.J. Garcí́a-Ripoll, and V.M. Pérez-Garcí́a, Phys. Rev. A **60**, 4864 (1999).

[17] D.L. Feder, C.W. Clark and B.I. Schneider, Phys. Rev. A **61**, 011601(R) (1999).

[18] D.L. Feder, C.W. Clark and B.I. Schneider, Phys. Rev. Lett. **82**, 4956 (1999).

[19] A.A. Svidzinsky and A.L. Fetter, Phys. Rev. Lett. **84**, 5919 (2000).

[20] N.K. Wilkin, J.M.F. Gunn, and R.A. Smith, Phys. Rev. Lett. **80**, 2265 (1998).

[21] D.A. Butts and D.S. Rokshar, Nature (London) **397**, 327 (1999).

[22] B. Mottelson, Phys. Rev. Lett. **83**, 2695 (1999).

[23] G.F. Bertsch and T. Papenbrock, Phys. Rev. Lett. **83**, 5412 (1999).

[24] G.M. Kavoulakis, B. Mottelson and C.J. Pethick, Phys. Rev. A **62**, 063605 (2000).

[25] N.K. Wilkin and J.M.F. Gunn, Phys. Rev. Lett. **84**, 6 (2000).

[26] M. Linn and A.L. Fetter, Phys. Rev. A **60**, 4910 (1999).

[27] O.K. Vorov, M.S. Hussein and P. Van Isacker, Phys. Rev. Lett. **90**, 200402 (2003).

[28] O.K. Vorov, P. van Isacker, M.S. Hussein, and K. Bartschat, Phys. Rev. Lett. **95**, 230406 (2005).

[29] M. Manninen, S. M. Reimann, M. Koskinen, Y. Yu and M. Toreblad, Phys. Rev. Lett. **94**, 106405 (2005).

[30] M. Toreblad, M. Borgh, M. Koskinen, M. Manninen, and S. M. Reimann, Phys. Rev. Lett. **93**, 090407 (2004).

[31] V. Schweikhard, I. Coddington, P. Engels, V. P. Mogendorff, and E. A. Cornell, Phys. Rev. Lett. **92**, 040404 (2004).

[32] M. Manninen, S. Viefers, M. Koskinen, S.M. Reimann, Phys. Rev. B **64**, 245322 (2001).

[33] I. Romanovsky, C. Yannouleas and U. Landman, Phys. Rev. Lett. **93**, 230405 (2004).

[34] S.M. Reimann, M. Koskinen, M. Yu and M. Manninen, New J. Phys. **8**, 59 (2006).

[35] Gun Sang Jeon, Chia-Chen Chang, and J.K. Jain, J. Phys.: Cond. Mat. **16**, L271 (2004).

[36] Gun Sang Jeon, Chia-Chen Chang and J.K. Jain, Phys. Rev. B **69**, 241304(R) (2004).

[37] J.-P. Nikkarila and M. Manninen, cond-mat/0602386.

[38] N.R. Cooper and N.K. Wilkin, Phys. Rev. B **60**, R16279 (1999).

[39] M.S. Hussein and O.K. Vorov, Phys. Rev. A **65**, 0535603 (2002).

[40] M.S. Hussein and O.K. Vorov, Ann. Phys. (N.Y.) **298**, 248 (2002).

[41] M.S. Hussein and O.K. Vorov, Phys. Rev. A **65**, 053608 (2002).

[42] J.R. Grover, Phys. Rev. **157**, 832 (1967).

[43] A. Bohr, and B. R. Mottelson, *Nuclear Structure*, Benjamin, New York (1969).

[44] A.H. MacDonald, Yang, S.R.E., & Johnson, M.D., Aust. J. Phys. **46**, 345 (1993).

[45] Reimann, S.M., and Manninen, M., Rev. Mod. Phys. **74**, 1283 (2002).

[46] R.B. Laughlin, Phys. Rev. B **27**, 3383 (1983).

[47] T. Stopa, B. Szafran, M.B. Tavernier and F.M. Peeters, Phys. Rev. B **73**, 075315 (2006).

[48] A.D. Güçlü and C.J. Umrigar, Phys. Rev. B **72**, 045309 (2005).

[49] A.D. Güçlü, Gun Sang Jeon, C.J. Umrigar and J.K. Jain, Phys. Rev. B **72**, 205327 (2005).

[50] A.G. Morris and D.L. Feder, cond-mat/0602037.

[51] M. Stone, H.W. Wyld, and R.L. Schult, Phys. Rev. B **45**, 14156 (1992).

[52] R.B. Lehoucq, D.C. Sorensen, and Y. Yang, "ARPACK User's guide: Solution to Large Scale Eigenvalue Problems with Implicitly Restarted Arnoldi Methods", FORTRAN code http://www.caam.rice.edu/software/ARPACK

[53] S.A. Trugman and S. Kivelson, Phys. Rev. B **31**, 5280 (1985).

[54] P.A. Maksym and T. Chakraborty, Phys. Rev. Lett. **65**, 108 (1990).

[55] P.A. Maksym, Phys. Rev. B **53**, 10871 (1996).

[56] M. Koskinen, M. Manninen, B.R. Mottelson, and S.M. Reimann, Phys. Rev. B **63**, 205323 (2001).

[57] S. Viefers, P. Koskinen, P. Singha Deo, M. Manninen, Physica E **21**, 1 (2004).

[58] A. Wójs and P. Hawrylak, Phys. Rev. B **56**, 13227 (1997).

[59] A.D. Jackson, G.M. Kavoulakis, B. Mottelson and S.M. Reimann, Phys. Rev. Lett. **86**, 000945 (2001).

[60] H. Saarikoski and A. Harju, Phys. Rev. Lett. **94**, 246803 (2005).

[61] M. Toreblad, Y. Yu, S.M. Reimann, M. Koskinen and M. Manninen, to be published (2006).

[62] S.-R. Eric Yang and A.H. MacDonald, Phys. Rev. B **66**, 041304(R) (2002).

[63] M. Tinkham, *Group theory and quantum mechanics* (McGraw-Hill, New York 1964).

[64] G.M. Kavoulakis, S.M. Reimann and B. Mottelson, Phys. Rev. Lett. **89** 079403 (2002).

[65] S. Viefers, H. Hansson and S.M. Reimann, Phys. Rev. A **62**, 53604 (2000).

[66] C. Chang, N. Regnault, T. Jolicoeur, and J.K. Jain, Phys. Rev. A **72**, 013611 (2005).

[67] N. Regnault and Th. Jolicoeur, Phys. Rev. Lett. **91**, 030402 (2003).

[68] N. Regnault and Th. Jolicoeur, Phys. Rev. Lett. **69**, 235309 (2004).

[69] J.K. Jain, and R.K. Kamilla, in *Composite Fermions: A unified view of the quantum Hall effect*, edited by O. Heinonen (World Scientific, River Edge, NJ, 1998).

[70] M.N. Korslund, and S. Viefers, cond-mat/0602620. (2005).
[71] V. Ruuska and M. Manninen, Phys. Rev. B **72**, 153309